Adjoint Physics in a Nonhydrostatic Mesoscale Adjoint Modeling System

X. Zou

National Center for Atmospheric Research
P.O. Box 3000, Boulder, CO 80307

Abstract

An adjoint model of the PSU/NCAR Mesoscale Model version 5 (MM5) has recently been developed and tested. It includes two cumulus parameterization schemes, an explicit microphysical parameterization scheme and two planetary boundary layer (PBL) schemes (a bulk parameterization and a high-resolution model of planetary boundary layer).

As an illustration of the feasibility of using a model with adjoint physics, we present results from a rainfall assimilation experiment. The impact of adjoint physics is investigated, the restriction of the rainfall assimilation is discussed, differences in the adjoint sensitivity results are presented, and the computational requirement for the data assimilation with adjoint physics is provided. The MM5 adjoint model with full-physics is shown to be accurate, user-friendly, and capable of being applied to mesoscale research. We also carefully examined the accuracy of the MM5 tangent linear model with and without moist physics by comparing its results with those produced by identical perturbations introduced into the nonlinear MM5 forecasts.

1. Introduction

Mesoscale numerical weather prediction requires a complete and accurate specification of the three-dimensional structure of the atmosphere at the initial time. Traditional upper-air soundings, which are available at 12-h intervals and 400-500 km apart, are not sufficient to properly define the initial conditions for a mesoscale model. The emergence of new observing systems (such as the GOES/8-9, NEXRAD, ACARS, GPS/MET, wind profiler, ...etc) provides a unique opportunity to improve the quality of initial conditions. However, many of these new observing systems provide non-traditional measurements (such as radiance or radio refractivity) at asynoptic times. Moreover, each of these systems has its own

measurement and error characteristics. An effective data assimilation procedure is needed in order to extract useful meteorological information from the raw measurements.

The four-dimensional variational data assimilation scheme (4DVAR), which employs the adjoint techniques, is one of the most promising approaches. The objective of 4DVAR is to find an "optimal" initial condition (IC) that will result in a 4-dimensional (4-D) model solution which best fits various observations distributed within a certain time and space interval. The 4-D structure of the model solution shall provide a more consistent and coherent description of the atmosphere than the observations which are incomplete most of the time. An improved model forecast starting from the "optimal" IC can also be expected. The tangent linear model (TLM) and adjoint model of a given forecast model that are developed in 4DVAR can also be applied to other studies such as sensitivity analysis and singular vector calculation which help address the stability and predictability issues.

Despite the importance of 4DVAR in large-scale and mesoscale prediction, active research in 4DVAR is still largely limited to a use of an adiabatic model with or without simple physics. It is now generally recognized that physical parameterization processes should be included in the 4DVAR system to increase the realism of the numerical model and to best assimilate new types of indirect observations which have a strong relation to moist physics and surface processes.

Over the past three years, the MM5 TLM and adjoint model with complex physics have been developed. In this paper, some issues related to the adjoint physics in the MM5 adjoint modeling system will be addressed. We present a 4DVAR experiment assimilating 3-h rainfall using a full-physics adjoint model including a microphysics scheme, a cumulus parameterization scheme, and surface fluxes. The impact of physics on the 4DVAR results is assessed, and the computational expenses is provided. We also discussed the accuracy of TLM with moist physics.

2. Adjoint model and experiment design

The full-physics MM5 adjoint model includes model dynamics, diffusion, two PBL schemes (bulk planetary-boundary-layer processes and Blackadar high-resolution PBL scheme), surface radiation, surface friction, a semi-implicit time-split integration scheme,

dry convective adjustment, two cumulus parameterization schemes (a Kuo-type cumulus parameterization scheme and the Grell scheme), resolvable-scale precipitation processes including large-scale precipitation and a microphysical scheme (Grell et al., 1993).

In a series of 4DVAR experiments conducted in Zou and Kuo (1996), a version of MM5 and its adjoint including large-scale precipitation and cumulus parameterization were used. The 4DVAR procedure, which incorporated 3-h rainfall data along with wind, temperature, surface moisture, and precipitable water measurements, not only fit the observations including rainfall, but also produced an improved short-range rainfall prediction. With the availability of the adjoint of a microphysics scheme and surface fluxes, additional 4DVAR experiments are conducted to further test the system and to assess the impact of mocrophysics. In the following, we will summarize these new results following the work by Zou and Kuo (1996).

The objective function is defined as:

$$
\begin{aligned}
J(\mathbf{x}(t_0)) = \sum_{r=0,R} \Big[& \mathbf{W}_u \left(\mathbf{u}(t_r) - \mathbf{u}^{obs}(t_r)\right)^2 + \mathbf{W}_v \left(\mathbf{v}(t_r) - \mathbf{v}^{obs}(t_r)\right)^2 \\
& + \mathbf{W}_T \left(\mathbf{T}(t_r) - \mathbf{T}^{obs}(t_r)\right)^2 \\
& + \mathbf{W}_{q_s} \left(\mathbf{q_s}(t_r) - \mathbf{q_s}^{obs}(t_r)\right)^2 + \mathbf{W}_{pw} \left(\mathbf{Qq}(t_r) - \mathbf{pw}^{obs}(t_r)\right)^2 \Big] \\
& + \mathbf{W}_r \left(\sum_{n=0}^{N} \mathbf{rx}(t_n) - \mathbf{R}^{obs}(t_R) \right)^2
\end{aligned}
\tag{2.1}
$$

which measures the distance between the model-predicted and observed wind, temperature, surface specific humidity fields, PW and the 3-h rainfall at time t_0 (1800 UTC) and t_R (2100 UTC). The term at t_0 serves as the simplest approximation to the actual background term. For detailed explanation of (2.14), see Zou and Kuo (1996).

First, we conducted three 4DVAR experiments minimizing the same cost function as that defined in (2.1) using three versions of the MM5 adjoint models: (1) E1.mcs includes microphysical scheme, cumulus parameterization, and surface flux; (2) E2.lc includes large-scale precipitation and cumulus parameterization; and (3) E3.dry uses only an adiabatic verson of MM5. After each minimization procedure was carried out over the 3-h window from 1800 UTC to 2100 UTC 10 April for 30 iterations, an 18-h model forecast using the same version of the model as that in E1.mcs was followed. A forward run starting from the

analysis at 1800 UTC 10 April without a data assimilation (E0.ctrl) was also conducted to provide a benchmark.

Secondly, two more 4DVAR experiments were carried out to see if the minimization procedure could produce precipitation over a region where there was no precipitation predicted in the control run (E0.ctr). This is motivated by the concern that the "on-off" switches associated with the precipitation processes are determined by the nonlinear model solution (Zou, 1996). Intuitively, it is easy to expect that rainfall data assimilation could correct the rainfall amount or to reduce the area of model predicted rainfall according to the observations. However, if the forward model did not produce rainfall, all those switches related to the moist processes will be kept off in the adjoint model. In such a situation, it is not clear how the observed rainfall information can impact the adjoint-model-derived gradient and then modify the model initial condition accordingly.

For all the experiments conducted in this paper, the LBCs are fixed. Since the 4DVAR code has undergone major revisions, mostly for code cleaning up, after we finished the paper by Zou and Kuo (1996), all the experiments are carried out using the same cleaned version of the 4DVAR code. Thus the experiment E2.lc, same as VTPWR.IC in Zou and Kuo (1996), is repeated to avoid the impact of possible inconsistency between the current and previous versions of the MM5 adjoint model on the 4DVAR results.

3. Numerical results

3.1 Minimization with additional adjoint physics

In Zou and Kuo (1996), experiments were conducted to assess the impact of the optimal control of LBCs, the importance of the precipitable water measurements to the rainfall assimilation, and the impact of using different cumulus parameterization schemes for assimilation. Here, we will first examine whether including a more complex grid-resolvable precipitation microphysics scheme and surface fluxes into the assimilation model could improve the 4DVAR results further. Then two additional rainfall assimilation experiments were conducted to examine whether the "observed" rain over a no-rain region can be assimilated into the model. Such a question arises from the fact that the "on-off" switches which control the adjoint of precipitation in the MM5 adjoint model were determined by the basic state.

Figure 1 shows the variations of the norm of the gradient of J with respect to the

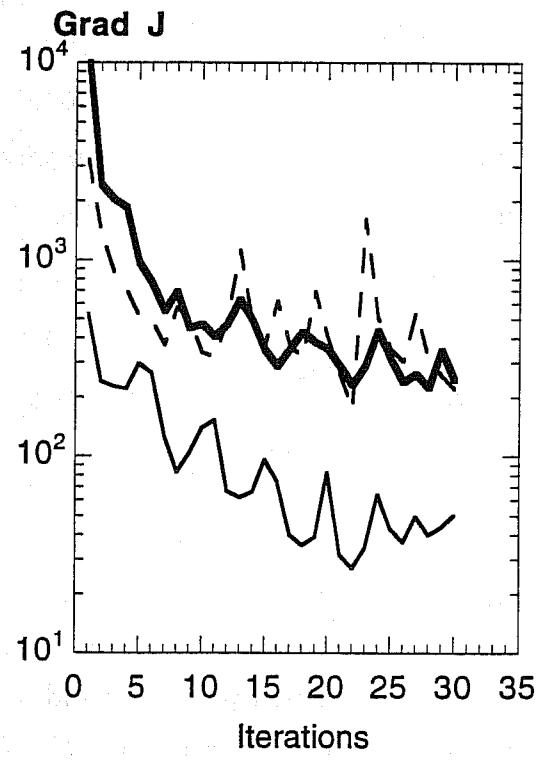

Figure 1: Variations of the norm of the gradient of J with respect to the initial condition for experiments E1.mcs (heavy solid line), E2.cl (thin dashed line), and E3.dry (thin solid line).

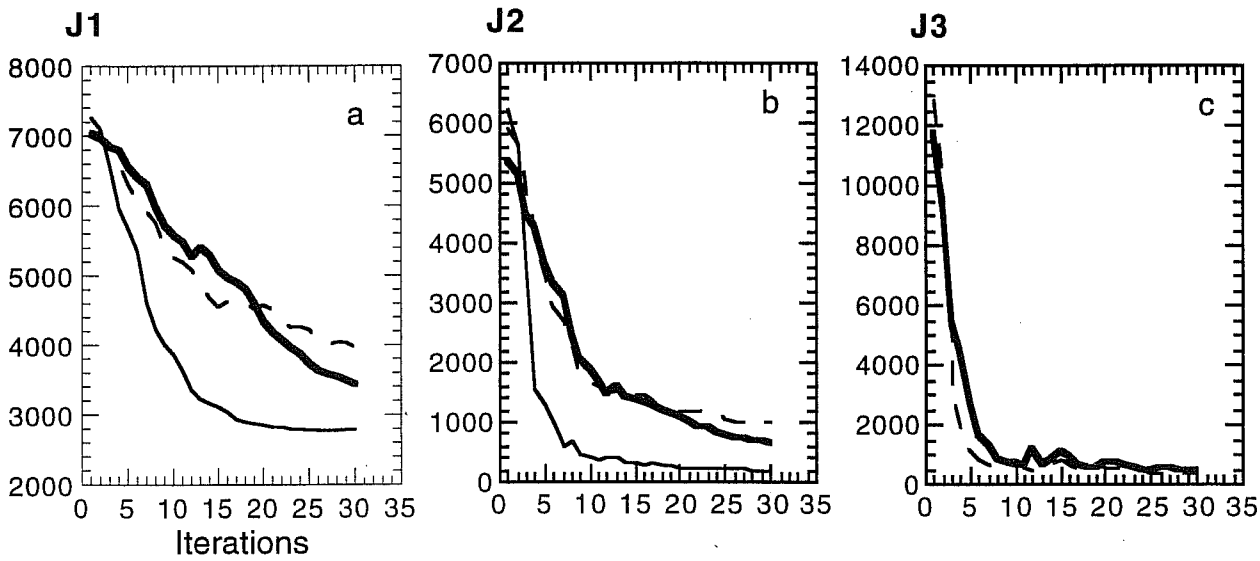

Figure 2: Variations of the cost function with the number of iterations for experiments E1.mcs (heavy solid line), E2.cl (thin dashed line), and E3.dry (thin solid line). (a) J_1 representing the distance between model predicted and analyzed wind, temperature and surface specific humidity (direct observations), (b) J_2 representing the PW difference between model prediction and analysis, and (c) J_3 representing the rainfall difference.

initial condition. A decrease between 1 or 1.5 orders of magnitude was obtained in all the three experiments: E1.mcs (thick solid), E2.lc (dashed), and E3.dry (thin solid). In order to see how the distances between model solution and observations are reduced, we show in Fig. 2 the variations of the cost function with the number of iterations. J is broken into three terms: J_1 represents the distance between model predicted and analyzed wind, temperature and surface specific humidity (see (3.1)), J_2 the PW difference between model prediction and analysis, and J_3 the rainfall difference. We found that with a dry model, the assimilation produced a closer fit to the analysis as reflected in the J_1 and J_2 terms. There is not much difference between E1.mcs and E2.lc as far as the fit to the observations is concerned. Most changes seem to occur within the first 10 iterations for the J_2 and J_3 terms, but the adjustment for the J_1 term seems to last longer. The question we would like to ask is (i) what happens to the rainfall prediction and (ii) how different is the adjustment in the initial condition using different physics adjoints?

Figure 3 shows the threat scores of the 3-h rainfall for all of the three assimilation experiments as verified against the observations. The results for the precipitation thresholds ranging from 0 mm to 10 mm are presented for the 3-h rainfall prediction during (a) 1800-2100 UTC 10 April and (b) 2100 UTC 10 to 0000 UTC 11 April. We found that experiments E1.mcs (heavy solid line) and E2.lc (thin dashed line) produced a similarly improved rainfall prediction and E.ctrl (dotted line) produced the lowest score of the 3-h rainfall prediction. The assimilation experiment E3.dry without rainfall data (thin solid line) produced a much improved rainfall prediction than that in E0.ctrl, which represents a similar difference between E0.ctrl and the forecast starting from analysis at 2100 UTC 10 April, the ending time of the assimilation (Figure omitted). One conclusion we can draw from this is that adding a microphysics scheme and surface fluxes to the assimilation does not produce much difference for the rainfall prediction. Part of the reason is that most of the rain in this case is convective rain and the vertical resolution (10 levels total) near the surface is rather poor. However, having the adjoints of microphysics and surface fluxes does not degrade the results either.

Figure 4 shows for example the adjustment obtained in E3.dry (left column) and E1.mcs (right column) for the 500-mb temperature and 850-mb specific humidity fields. A larger adjustment is found in the "optimal" IC in E3.dry than in E1.mcs. The rain-related change of temperature and specific humidity fields from 1800 UTC to 2100 UTC

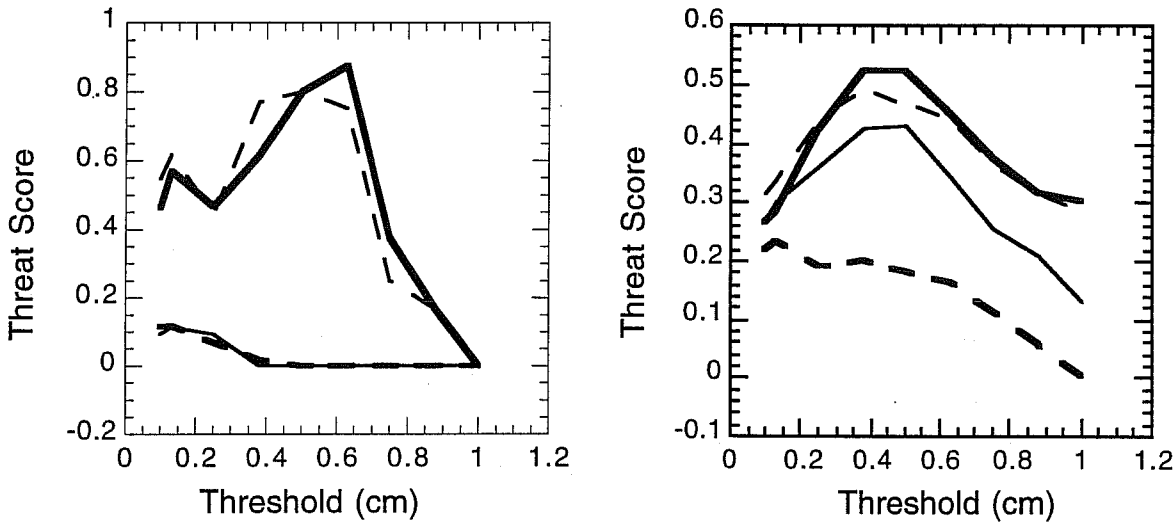

Figure 3: The threat scores of the 3-h rainfall for all of the assimilation experiments E1.mcs (heavy solid line), E2.cl (thin dashed line), and E3.dry (thin solid line), verified against the observations.

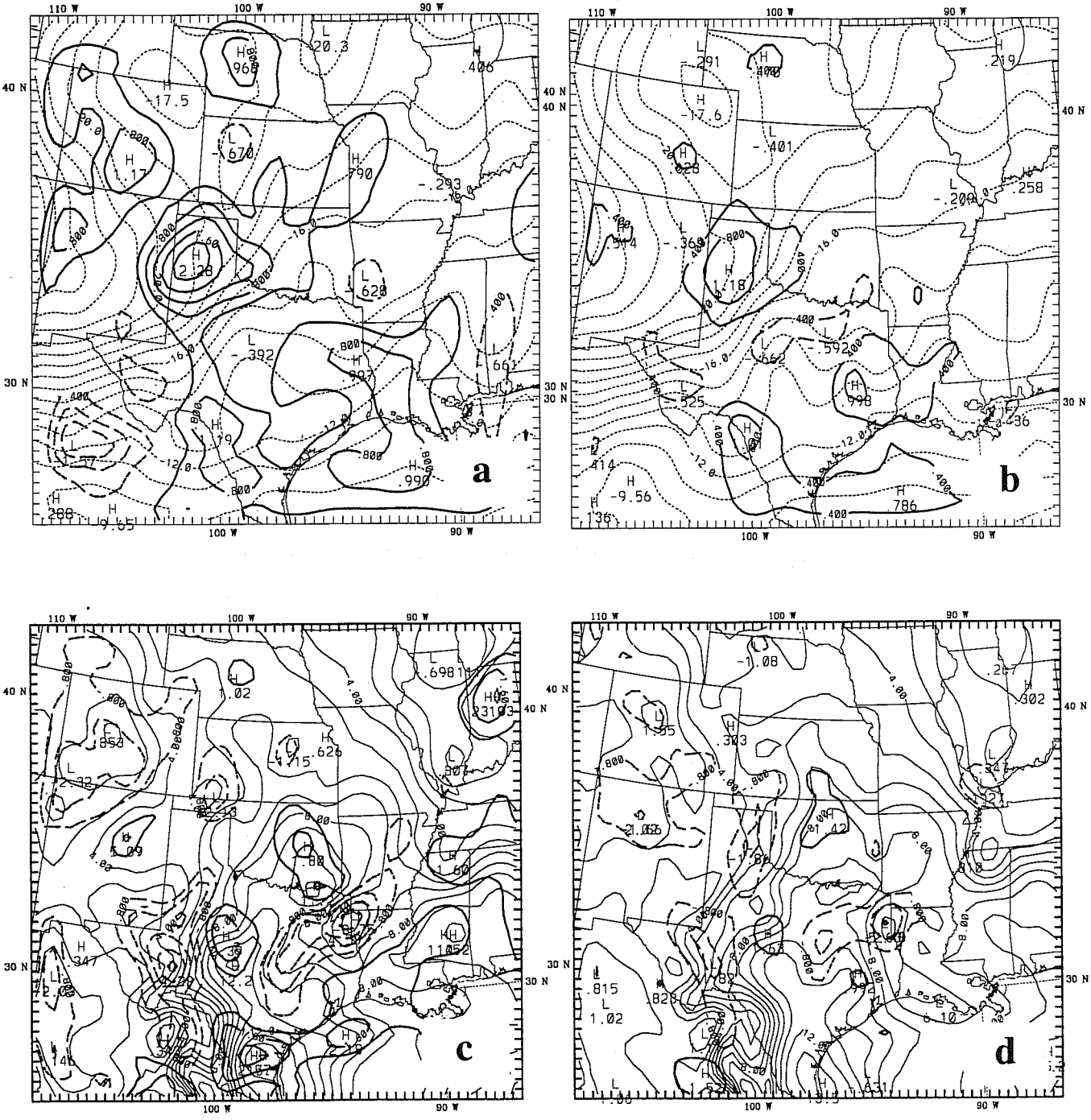

Figure 4: The adjustment obtained in E3.dry (left column) and E1.mcs (right column) for the 500-mb temperature (a-b) and 850-mb specific humidity (c-d) fields. Thin lines represent the "optimal" ICs and solid lines the differences between E3.dry and E0.ctrl (left) and E1.mcs and E0.ctrl (right). Contour intervals are 1°C for the 500-mb temperature, 0.4°C for the 500-mb temperature difference, 1 g/kg for the 850-mb specific humidity, and 0.8 g/kg for the 850-mb specific humidity difference.

are reflected in the "optimal" IC obtained using a dry MM5 model. The latent heat release associated with the observed 3-h rainfall, which is missing in the dry run, is reflected in the adjusted IC in E3.dry in which a maximum value of 2.28°C temperature adjustment is observed over the Texas Panhandle. This value is 1.1°C higher than that in E1.mcs. The modifications in the moisture field in E1.mcs is only 1/3 of that in E3.dry. The maximum of 4.79 g/kg adjustment to the analysis is produced in E3.dry while in E1.mcs the maximum value is only 1.82 g/kg. It seems that in order to produce a similar fit to the observations of u, v, T, PW, and q_s at 2100 UTC 10 April, the minimization procedure using a dry model will produce too large a change in the IC at 1800 UTC 10 April to compensate some of the model errors due to the missing physics. The adjustment to the analysis at 1800 UTC 10 April in E2.cl is found to be similar to those in E1.mcs (Figure omitted). More discussions on the modification to the ICs made by 4DVAR can be found in Zou and Kuo (1996).

The model was run at 40-km resolution with a grid size of 49x55x10. For 30 iterations of the 3-h assimilation with a time step of 120s, E1.mcs used 57785 CPU seconds and 11.33 MW memory on a Cray J90 machine. It is reduced to 47223 seconds and 11.32 MW in E2.lc and 43856 seconds and 11.32 MW in E3.dry. The large CPU requirement results from the expensive MM5 adjoint model integration which is not yet optimized or parallelized, and with many repeated calculations of the basic-state dependent coefficients. The later is caused by the j-slice structure of MM5 and a rule we set for MM5 adjoint model that only the model states at every time step are saved and all the intermediate variables are recalculated in the MM5 TLM and adjoint model. A preliminary test of the optimization of MM5 adjoint model shows that the CPU time can be reduced by half.

3.2 Assimilating rainfall data over a no-rain region

Model moist physics contains "on-off" switches. These switches are retained in the assimilation model, and the TLM and adjoint model follow the same route as in the original nonlinear model, i.e., the switches are turned on or off based on the basic state solution around which the linearization was carried out (Zou, 1996). Convection is turned on when several criteria are satisfied (several switches are turned on). It is thus easy to expect that the model-predicted rainfall can be increased or decreased through rainfall assimilation over regions where the control forecast without data assimilation predicts rain, since those moist switches are activated in the forward and backward model integrations. But it is

unclear whether the 4DVAR procedure could fit the observed precipitation over regions where the control forecast, starting from the guess initial condition, doesn't produce rain.

Figure 5, for instance, shows the observed (dotted line) and model predicted (solid line) 3-h rainfall without data assimilation (E0.ctrl) during 1800 UTC and 2100 UTC 10 April. Even though both the location and the areal coverage are different, the observed rain is embedded in the general area where the model produced rain. After 3-h rainfall data assimilation, including the no-rain information contained in the observed rain distribution, the model starting from the adjusted initial condition, produced a remarkably similar rainfall distribution as observation (see Fig. 2 in Zou and Kuo, 1996). It will be interesting to see if we move the observed rain from its original place to a no-rain area, say near the point A, will 4DVAR able to fit the shifted 3-h rainfall "observation"? To answer this question, we conducted an experiment similar to E2.lc, E4.lc.shiftR, except the observed 3-h rainfall (centered at the point i=24,j=23) is now shifted to point A (i=9,j=29) (see Fig. 5). Figure 6 shows the 3-h rainfall prediction after the 30 iterations of assimilation minimizing J defined in (3.15) with shifted 3-h rainfall (E4.lc.shiftR). We found that shifted 3-h rainfall over the region A was nicely reproduced by the model forecast starting from the "optimal" initial condition (Fig. 6a). Mpreover, the erroneous rainfall over northern Texas and southern Oklahoma was largely removed. However, since this is an artifically set rainfall, it did not persist into the subsequent forecast (Fig. 6b).

How is the rainfall information brought into the model state? Let's take a look at the Kuo cumulus scheme, for instance. As described in Zou (1996), three switches are imposed to determine which grid is capable of supporting convection. When all three criteria are satisfied (i.e., all three switches are turned on), the model temperature and specific humidity fields are modified according to the formula which is written as:

$$\begin{aligned} T_k^* &= T_k + \frac{L_v}{c_p}(1-b)gM_tN_h(\sigma_k) \\ q_k^* &= q_k + bgM_tN_m(\sigma_k) + V_{qf}(\sigma_k) \\ P^* &= (1-b)M_t \end{aligned} \tag{3.16}$$

where T_k, q_k and T_k^*, q_k^* are the temperature and specific humidity before and after convection occurred, and P^* is the convective rain produced at time t. For detailed explanation of notation, please see Grell et al. (1994) and Zou (1996).

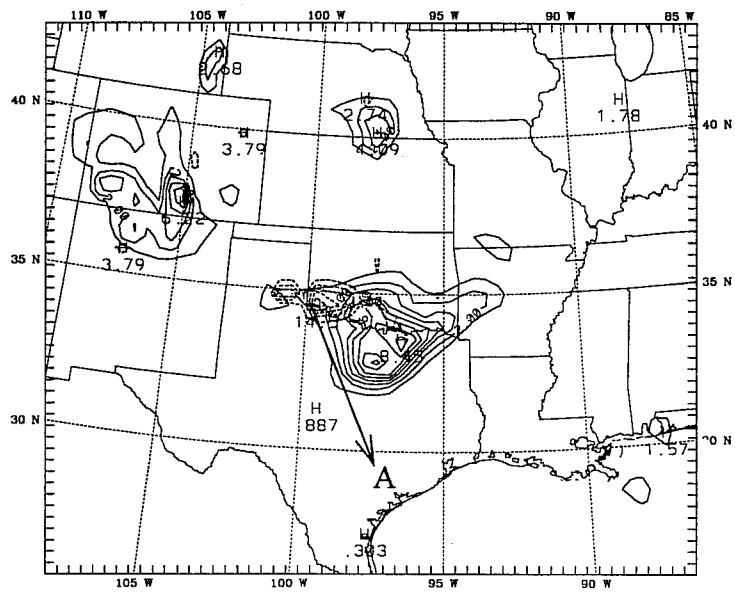

Figure 5: The observed (dotted line) and model predicted (solid line) 3-h rainfall without data assimilation (E0.ctrl) during 1800 UTC and 2100 UTC 10 April. Contour interval is 2.5 mm.

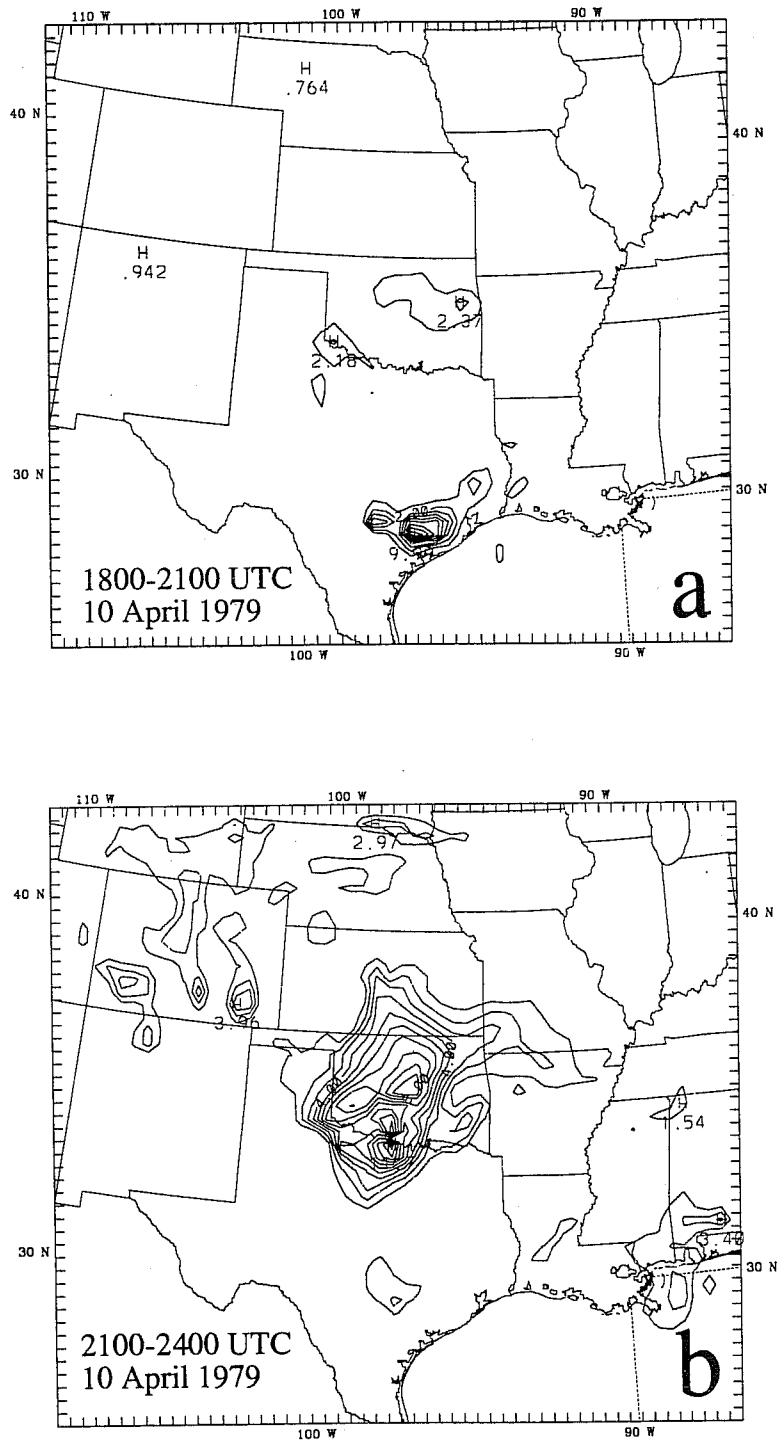

Figure 6: The 3-h rainfall prediction after the 30 iterations of assimilation with shifted 3-h rainfall (experiment E4.lc.shiftR). (a) 1800-2100 UTC 10 April 1979, and (b) 2100 UTC 10 to 0000 UTC 11 April 1979. Contour interval is 2.5 mm.

The adjoint operations corresponding to (3.16) can be written as

$$\begin{aligned}
\hat{M}_t &= (1-b)\hat{P}^* + bgN_m(\sigma_k)\hat{q}_k + \frac{L_v}{c_p}(1-b)gN_h(\sigma_k)\hat{T}_k \\
\hat{b} &= -M_t\hat{P}^* + gM_tN_m(\sigma_k)\hat{q}_k - \frac{L_v}{c_p}gM_tN_h(\sigma_k)\hat{T}_k \\
\hat{N}_m(\sigma_k) &= bgM_t\hat{q}_k \\
\hat{V}_{qf}(\sigma_k) &= \hat{q}_k \\
N_h(\sigma_k) &= \frac{L_v}{c_p}(1-b)gM_t * \hat{T}_k
\end{aligned} \tag{3.17}$$

where $\hat{F}$ represents the adjoint variable corresponding to the forward model variable F. Eq. (3.17) will only be executed if the convective criteria based on the nonlinear model solution are turned on.

As long as the model produces rain, which can be marginal, the switches that control the adjoint convection will be on, and the forcing measuring the discrepancy between model-predicted and observed rainfall:

$$2\mathbf{W}_r\left(\sum_{n=0}^{N}\mathbf{rx}(t_n) - \mathbf{R}_r^{obs}(t_R)\right) \tag{3.18}$$

will be added to the adjoint model variables through the adjoint operator of the rainfall calculation (3.17) with

$$\hat{P}^* = \mathbf{r}^T 2\mathbf{W}_r\left(\sum_{n=0}^{N}\mathbf{rx}(t_n) - \mathbf{R}_r^{obs}(t_R)\right), \tag{3.19}$$

at time t_n.

Through the relation of the adjoint convective rain variable with the adjoint moisture convergence $\hat{M}_t$ and the adjoint cloud fraction $\hat{b}$, the observed rainfall information will indirectly impact the adjoint variables of wind, temperature and specific humidity fields, which will then impact other model fields through model dynamics, numerics and physics. This information will be reflected in the gradient vector which provides the updated increment to the initial condition through a minimization procedure.

However, in a case when the model did not produce rain over an observed rain region, the observed rain information will not be able to impact the adjoint derived gradient

at the guess IC. This is because the switches for the adjoint operation of convective and non-convective precipitation, determined by the basic state trajectory, will be kept off in the backward adjoint model integration, as in the forward model. The forcing in (3.18) with $\sum_{n=0}^{N} \mathbf{rx}(t_n) = 0$ will have no way to impact the adjoint variables. This is true for the sensitivity study. In a 4DVAR experiment, it is not always true that the observed rainfall information over the forecast no-rain region can not be assimilated into the model. The explanation is as follows: As the model fits other observations (suppressing the precipitation over Texas and Oklahoma regions which are not observed), the model initial condition is changed. The new forecast may produce precipitation over a no-rain region of E0.ctrl, and the rainfall observation over the previous no-rain region will then have a way to impact the model state. This can be illustrated in Fig. 7 in which the 3-h rainfall values at the 9-model-grid points surrounding the center (point A in Fig. 5) of the shifted observed rainfall in E4.lc.shiftR A (i=9, j=29) in Fig. 5 are plotted as a function of iteration numbers.

We see from Fig. 7 that at the 0th iteration, none of the points had precipitation. However, after 1 iteration, precipitation occurred at point 1. After 2 iterations, both points 1 and 2 had non-zero precipitation. The model precipitation extended to points 3, 4, and 5 after 3 iterations. As more iterations were carried out, the precipitation region was further expanded south and westward. After 8 iterations, all the points except point 9 (see the low-left corner in Fig. 7) had non-zero precipitation. Figure 8 presents a more clear picture of how the model prediction of the 3-h rainfall was adjusted according to the observations. We observe that during the first two iterations, the major change was found in reducing the precipitation over the two main regions: one centered at the Oklahoma and Texas border, and the other centered at the Colorado and New Mexico border. The southern tip of the model precipitation over Texas was slightly extended southward, which connected with the "observed" rainfall region near point A. The western part of the observed rainfall information was first assimilated into the model in the 3rd and 4th iteration. In the following iterations, this small rainfall region extended south and northeastward, finally taking the shape of the "observed" 3-h rainfall distribution after 20 iterations. Most of the adjustment from no-rain to rain over the region A in Fig. 5 occurred during the first 8 iterations.

Next we carried out another rainfall assimilation in which the observed 3-h rainfall

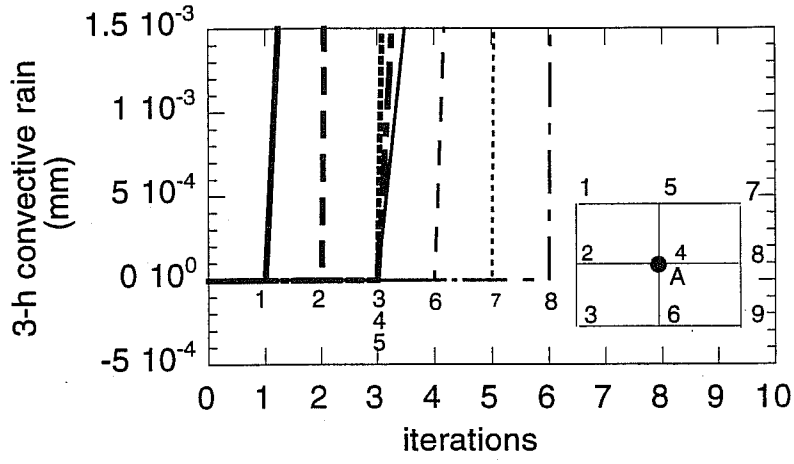

Figure 7: The values of the 3-h rainfall for the period of 1800 UTC and 2100 UTC 10 April at the 9-model-grid points surrounding the center (point A in Fig. 5) of the shifted observed rainfall at the point 1 (heavy solid line), point 2 (heavy dashed line), point 3 (heavy dotted line), 4th (heavy dash-dotted line), 5th (thin solid line), 6th (thin dashed line), 7th (thin dotted line), and 8th (thin dash-dotted line) iteration.

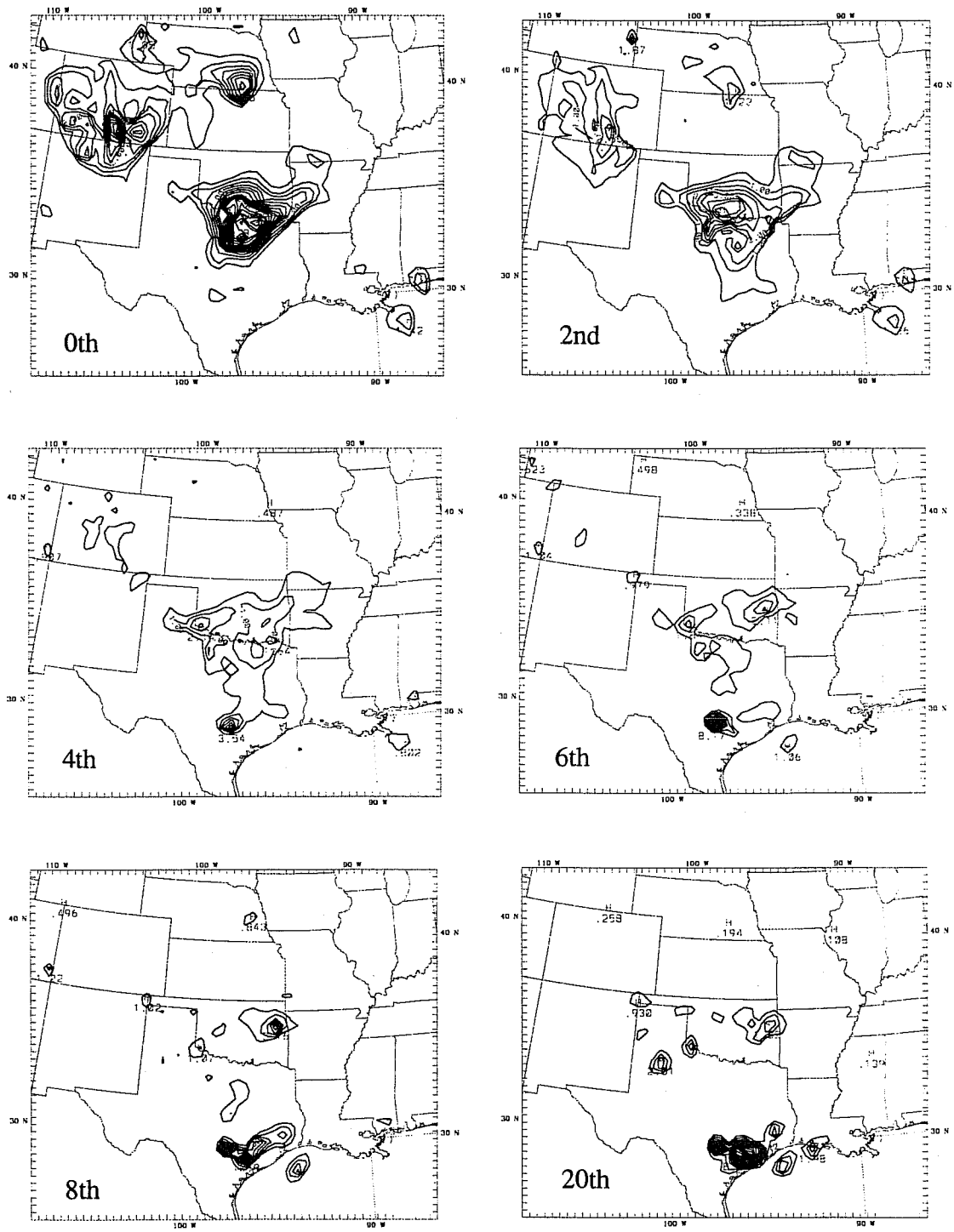

Figure 8: The model prediction of the 3-h rainfall from 1800 UTC to 2100 UTC 10 April 1979 at the 0th, 2rd, 4th, 6th, 8th and 20th iteration. Countour interval is 2.5 mm.

was shifted to the southwestern corner of the model domain over Mexico west of the dryline where there is no model precipitation nearby and the moisture content is low. The 4DVAR failed to produce the shifted rainfall over Mexico. It can be concluded that the observed rainfall over a region where the model produces no rain may or may not be incorporated into the model, depending on whether there are other observations which can adjust the model IC so that the new model forecast will produce precipitation during the entire minimization procedure. Otherwise, such rainfall observations cannot be assimilated into the model. One possible way to remedy this shortcoming in the variational rainfall data assimilation is to not include the basic-state based "on-off" switches in the forward observational operator. Another possibility is to use an incremental approach in which a more complex forward model is used for the basic state, which may produce a better rainfall coverage comparing to the observed rain. Further study in this direction is needed.

4. Nonlinearity and discontinuity

4.1 TLM approximation

The MM5 TLM is a model obtained by linearizing the MM5 around a nonlinear model solution. It is developed for a convenient construction of the MM5 adjoint model (see section 2.2). However, the MM5 TLM itself has several other important usages. For example, it can be used for singular vector calculation, for time-variant normal mode calculation, for an incremental variational data assimilation approach, and even in the Kalman filter for propagating error statistics. A TLM describes the evolution of the differences between two nonlinear model solutions when one solution begins from a perturbed initial condition and the other starts from an unperturbed initial condition. The TLM is correct and accurate if its solution approximates the difference of the two nonlinear model's solutions with increasing accuracy as the size of the initial perturbation tends toward zero.

For a finite initial perturbation, the degree to which the TLM solution approximates the evolution of the nonlinear model perturbation depends on the degree of nolinearity, and/or discontinuity if any, of the solution. Figure 9 shows the time evolution of the domain-averaged root-mean-square (rms) error of the perturbation solutions of the zonal wind (u), compared against the unperturbed nonlinear solution (basic state). It is calculated through the following formula:

$$rms_{\alpha}(t) = \frac{\|\mathbf{x}^{ptb}(t,\alpha) - \mathbf{x}(t)\|}{N} \tag{4.1}$$

where

$$\mathbf{x}^{ptb}(t,\alpha) = \mathbf{Q}_t(\mathbf{x})(\mathbf{x}_0 + \alpha(\mathbf{x}_0^{(30)} - \mathbf{x}_0)). \tag{4.2}$$

Here N is the dimension of model variable $\mathbf{x}$, $\mathbf{x}_0$ is the analysis at 1800 UTC 10 April, $\mathbf{x}_0^{(30)}$ is the "optimal" initial condition obtained in the experiment E1.mcs (see Section 2), and α is a real number with its values ranging from unit to 10^{-12} to control the magnitude of the initial perturbation. Therefore, the initial perturbation $\alpha\Delta\mathbf{x}_0$ $(= \alpha(\mathbf{x}_0^{(30)} - \mathbf{x}_0))$ is the difference between the "optimal" initial condition in E1.mcs (see Section 3.3) and the analysis at 1800 UTC 10 April 1979, multiplied by a factor of α which controls the magnitude of the initial perturbations.

We observe that for the adiabatic version of MM5 (Fig. 9a), the logarithmic rms error of the perturbed solution decreases linearly as the order of the magnitude of the initial perturbation (α) decreases. However, when moist processes (large-scale precipitation and the Kuo cumulus parameterization scheme) are included, the perturbation solution shows rapid error growth in the course of the integration for perturbations ranging from $\alpha = 10^{-2}$ to $\alpha = 10^{-6}$ (Fig. 9b). It is believed that this is a result of strong nonlinearity associated with the occurrence of the convective and non-convective precipitations. As the initial perturbation decreases further, the rms error again decreases logarithmically linearly with respect to $\log(\alpha)$. It seems that the TLM including moist physics will result in a much stronger nonlinearity than that for an adiabatic model.

The linear approximation to the difference between the perturbed and unperturbed nonlinear model solutions

$$\mathbf{x}^{ptb}(t,\alpha) - \mathbf{x}(t) \tag{4.3}$$

can be expressed as

$$\alpha\mathbf{P}_t\Delta\mathbf{x}_0, \tag{4.4}$$

which is a result of the TLM integration multiplied by α. We observe from (4.4) that as α decreases, the line pattern of the TLM solutions for various values of α will not change, though the magnitude of the TLM solutions will change as α is changed. Therefore, we can conclude from Fig. 9b, without actually examining the TLM solution, that the TLM including moist physics would not approximate the nonlinear perturbation well for initial perturbation ranging from $\alpha = 10^{-2}$ to $\alpha = 10^{-6}$, which are very small perturbations. This conclusion does not depend on how we coded the TLM model, i.e., whether we keep the

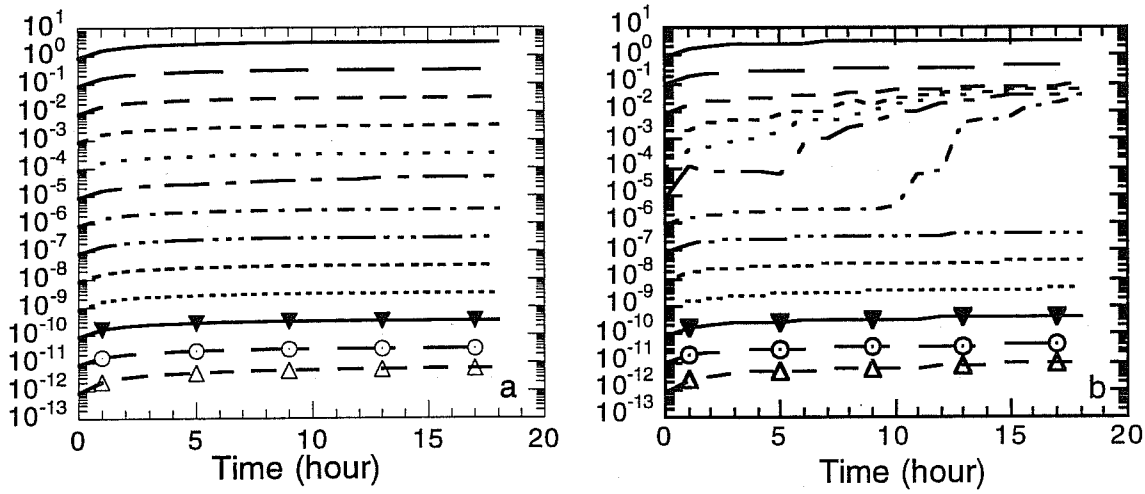

Figure 9: The time evolution of the domain-averaged root-mean-square (rms) errors of the perturbation solutions (with the values of α ranging from 10^0 to 10^{-12}) of the zonal wind (u), compared against the unperturbed nonlinear solution (basic state), using an adiabatic version of MM5 TLM (a) and a version of MM5 TLM with moist physics (b).

"on-off" switches the same as in the nonlinear model (Zou, 1996) or we would differentiate the switches themselves (Xu, 1995).

In order to compare the TLM results with that of nonlinear results, we show in Fig. 10 the rms error of the nonlinear model perturbation solution (solid) and that of the TLM solution for $\alpha = 10^{-10}$ with and without moist physical processes. The TLM solution is a very good approximation to the corresponding nonlinear perturbation solution even when the moist processes are included, although it is not true for $\alpha \leq 10^{-6}$. In the next subsection, we will make further diagnosis to the strong nonlinear behavior of the perturbation solutions observed in Fig. 9b when moist convection is included in the NLM for the range of α from $\alpha = 10^{-2}$ to $\alpha = 10^{-6}$.

5.2 Nonlinearity and discontinuity

In order to further examine the cause of strong nonlinear behavior of the perturbation solutions observed in Fig. 9b for $\alpha \leq 10^{-6}$, we would first like to see where the largest rms errors exist and why the rms errors become large after a few hours of integration for $10^{-2} \leq \alpha \leq 10^{-6}$? Is it a result of discontinuity or nonlinearity?

Fig. 11 shows the 6-h temperature forecast difference on 500 mb at 0000 UTC 11 April between the perturbed (E.10^{0}, E.10^{-1}, ..., E.10^{-7}) and unperturbed (E.noptb) NLM runs. If the time evolution of the model state is mostly linear, then the figures which plot the differences shall look similar if the contour intervals for E.10^{0} - E.noptb, E.10^{-1} - E.noptb, ..., and E.10^{-6} - E.noptb are adjusted accordingly (5×10^{-1} °C, 5×10^{-2} °C, ..., and 5×10^{-7} °C). This is not true as seen in Fig. 11 for $10^{-2} \leq \alpha \leq 10^{-4}$. For $\alpha \geq 10^{-5}$, we observe a similar pattern of the temperature difference, though the magnitude of the forecast differences decreases as that of the initial perturbation does.

The extremely large 6-h forecast differences in the temperature field (Figs. 11) for E.10^{-2}, E.10^{-3}, and E.10^{-4} occurred at the center of the domain. Over the rest of the domain, the forecast differences still show a linear behavior (see plot for E.10^{-2}). In order to confirm that such a strong nonlinear behavior in the model state is related to the precipitaion, we present in Fig. 12 the forecast differences of the 6-h convective rainfall ending at 0000 UTC 11 April for experiments E.10^{0}, E.10^{-1}, ..., and E.10^{-6}. It is clear that the large temperature differences occur over a region where excessive convective rain

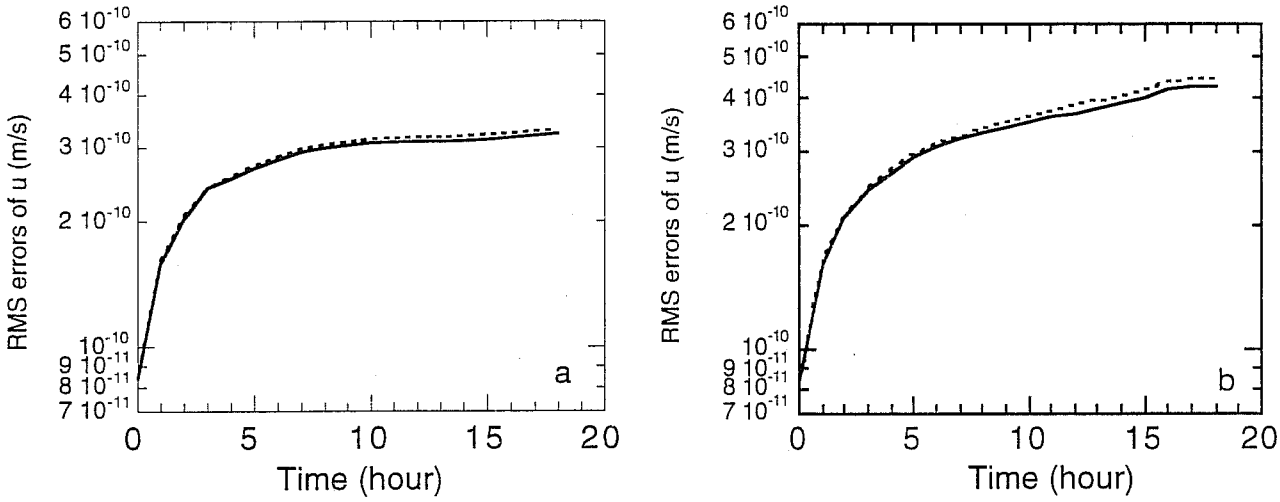

Figure 10: The rms error of the nonlinear model perturbation solution (solid) and that of the TLM solution for $\alpha = 10^{-10}$ (a) without and (b) with moist physical processes.

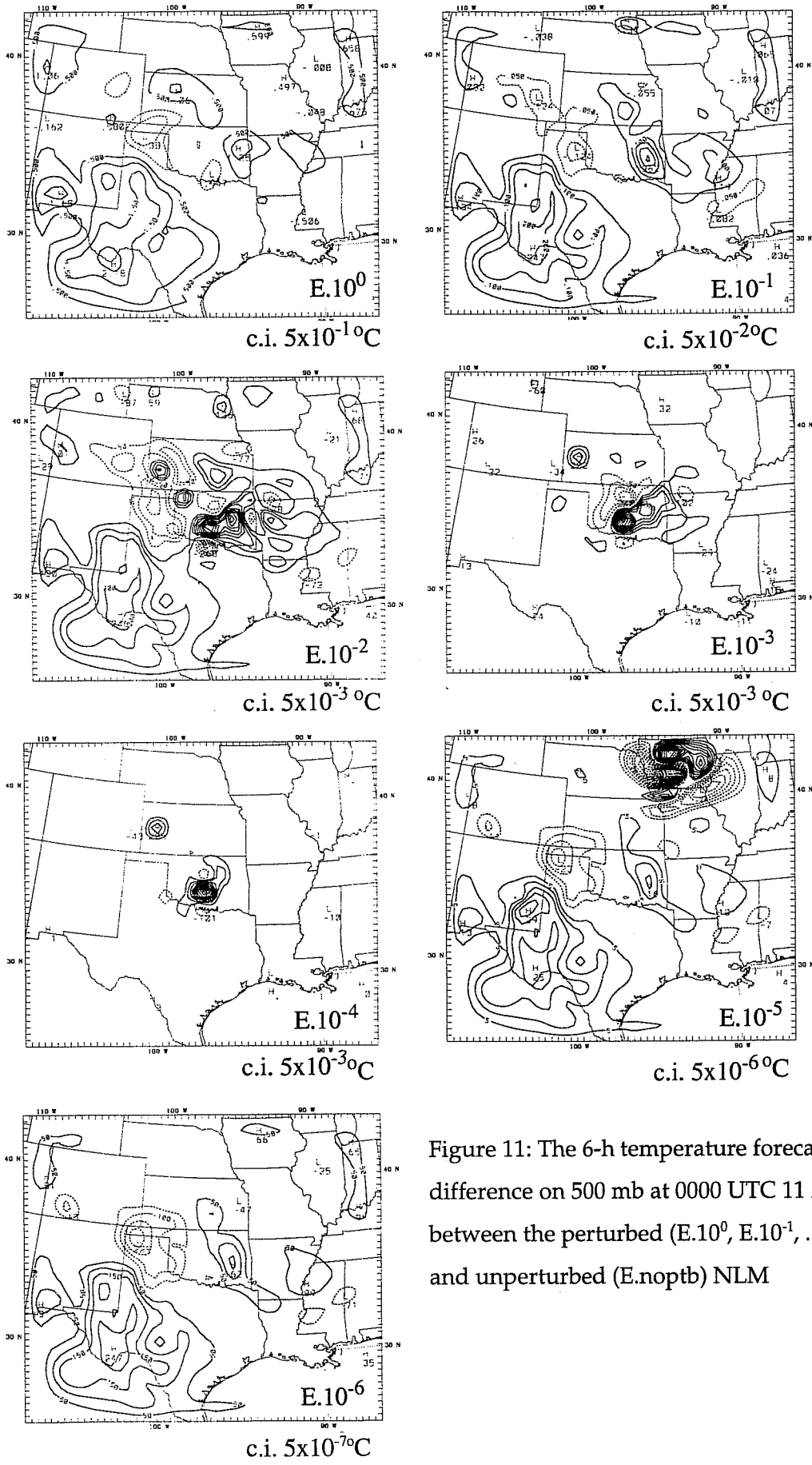

Figure 11: The 6-h temperature forecast difference on 500 mb at 0000 UTC 11 April between the perturbed ($E.10^0$, $E.10^{-1}$, ..., $E.10^{-7}$) and unperturbed (E.noptb) NLM

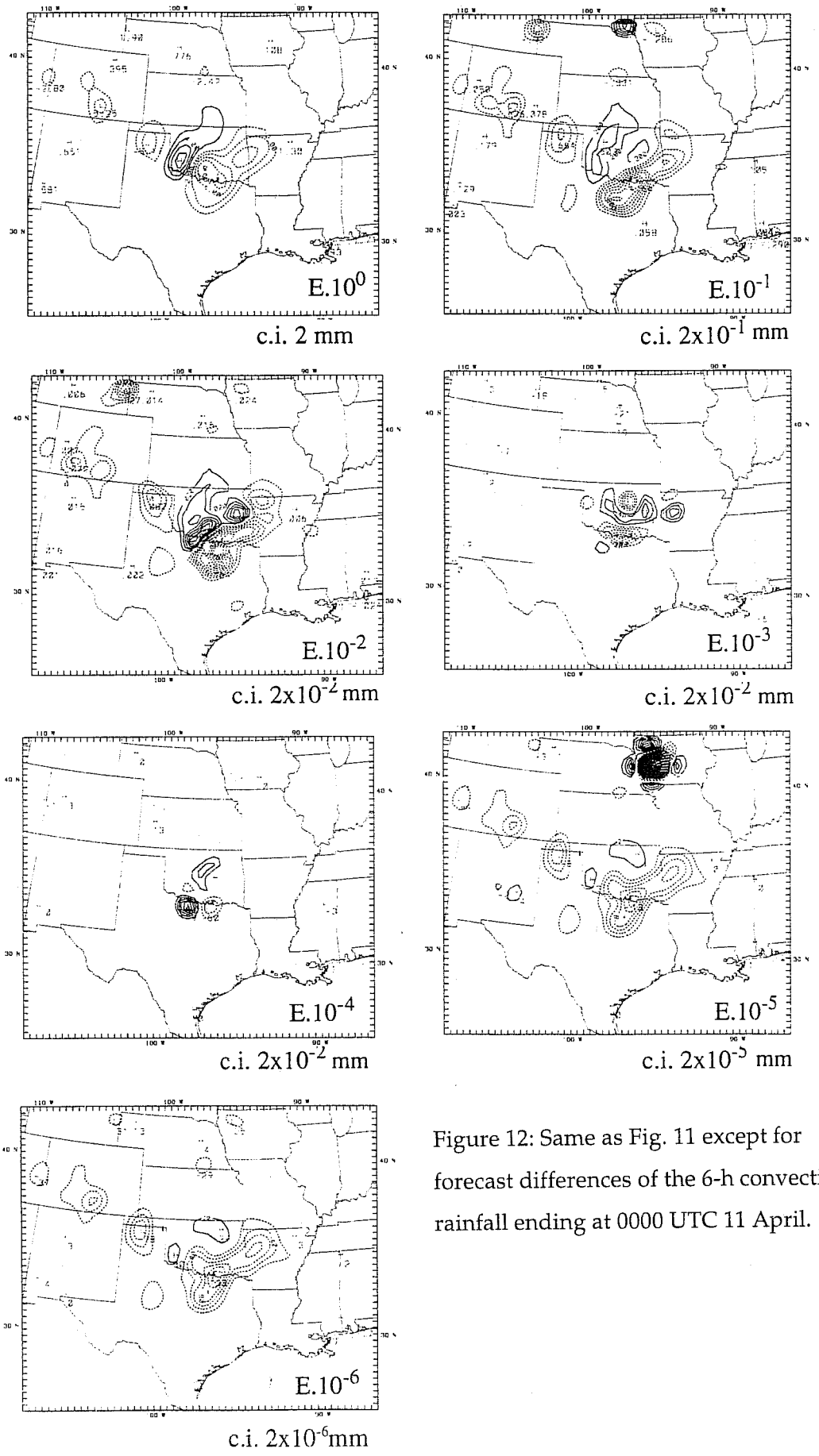

Figure 12: Same as Fig. 11 except for forecast differences of the 6-h convective rainfall ending at 0000 UTC 11 April.

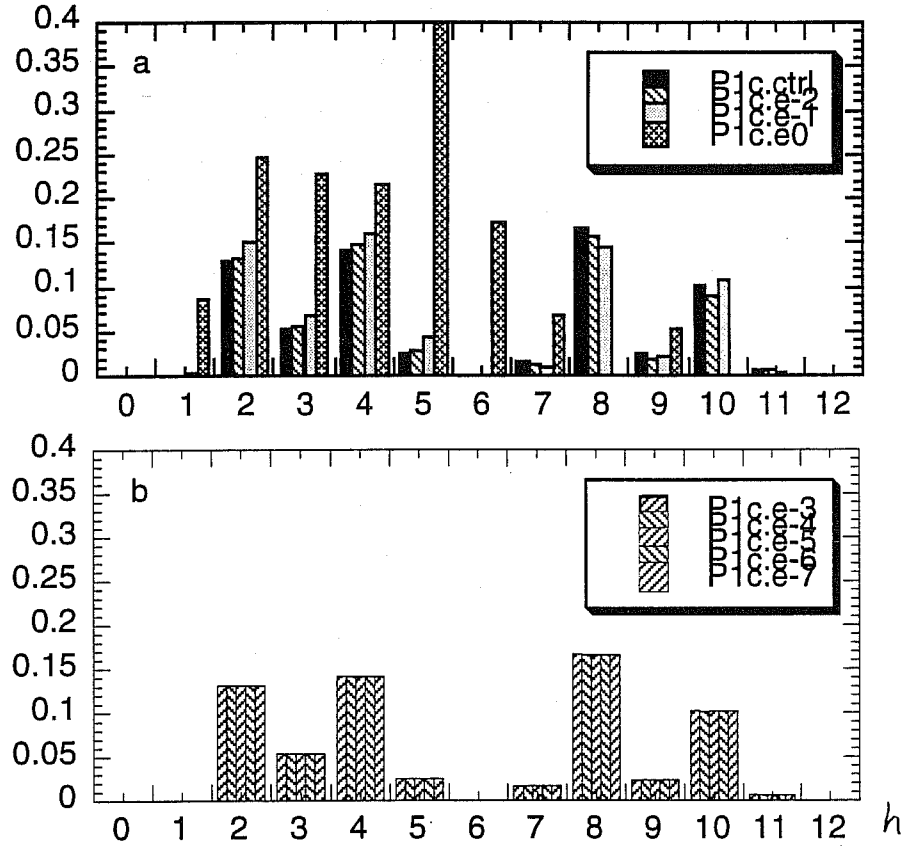

Figure 13: The hourly rainfall at the central point of the observed 3-h rainfall (see Fig. 5) for (a) experiments E.10^{-12}, E.10^{0}, E.10^{-1}, and E.10^{-2}, and (b) E.10^{-3}, E.10^{-4}, ..., and E.10^{-7}.

differences are observed. The 6-h rainfall differences for E.10^{-3} and E.10^{-4} reach a similar magnitude as that in E.10^{-2} between the perturbed and unperturbed runs, though the perturbation in ICs differs by an order of magnitude. Are these large forecast differences a reflection of the nonlinearity inherited in the convective scheme, or due to the presence of the "on-off" switches (discontinuity), or both?

We choose a convective point (i=24, j=24) centered at the observed 3-h rainfall (see Fig. 5) to plot its hourly rainfall (Fig. 13) and the time evolution of the perturbed convective rainfall difference (Fig. 14) for experiments E.10^{0}, E.10^{-1}, ..., and E.10^{-7}. This represents a situation where the convection is enhanced if the IC (analysis) is perturbed with $\alpha = 1$ (equivalent to the "optimal" IC obtained in the experiment E1.mcs in section 3). The unperturbed run can be viewed as a perturbed run with a very small value of $\alpha = 10^{-12}$ in this case (equivalent to the experiment E0.ctrl in section 3.3). Adjustment in the convectivity from that in the perturbed run E.10^{0} to that in the weakly perturbed run E.10^{-12} (equivalent to E.noptb) has to occur when the value of α is decreased from 1 to 10^{-12}. The hourly convective rainfall shall approximately show how differently the convective "on-off" switches are turned on or off, and the time evolution of the perturbed convective rainfall difference shall reveal the degree of nonlinearity in the cumulus scheme.

We found from Fig. 13 that the hourly rainfall produced by the perturbed nonlinear model is significantly different for E.10^{0}, E.10^{-1}, and E.10^{-2}. When α is equal to 10^{-3} or smaller, the hourly rainfalls at the same point are all the same. However, in Fig. 14 we observe a very different behavior for the time evolution of the hourly convective rain as the order of magnitude of the initial perturbation is decreased, especially for the range of α from 10^{-3} to 10^{-7} (Fig. 14d to Fig. 14h). For those experiments in which α is smaller than 10^{-7}, the perturbed forecast produced the same amount of hourly convective rain. It is from this value of α (=10^{-7}) and smaller that the rms errors of the perturbed runs show a linear evolution of the solution with respect to α (see Fig. 9b), as was observed in the adiabatic model (Fig. 9a). We also examined several other convective points: (21,30), (21,28), (24,28), and (27,28) and similar results are obtained (Figures omitted). We thus conclude that the strong nonlinear behavior observed in Fig. 9b for $\alpha \leq 10^{-6}$ is mainly a result of the strong nonlinearity contained in the moist physics. If the perturbed nonlinear solution produces a rainfall prediction different from that in the control simulation (unperturbed run), stronger nonlinear behavior can be expected

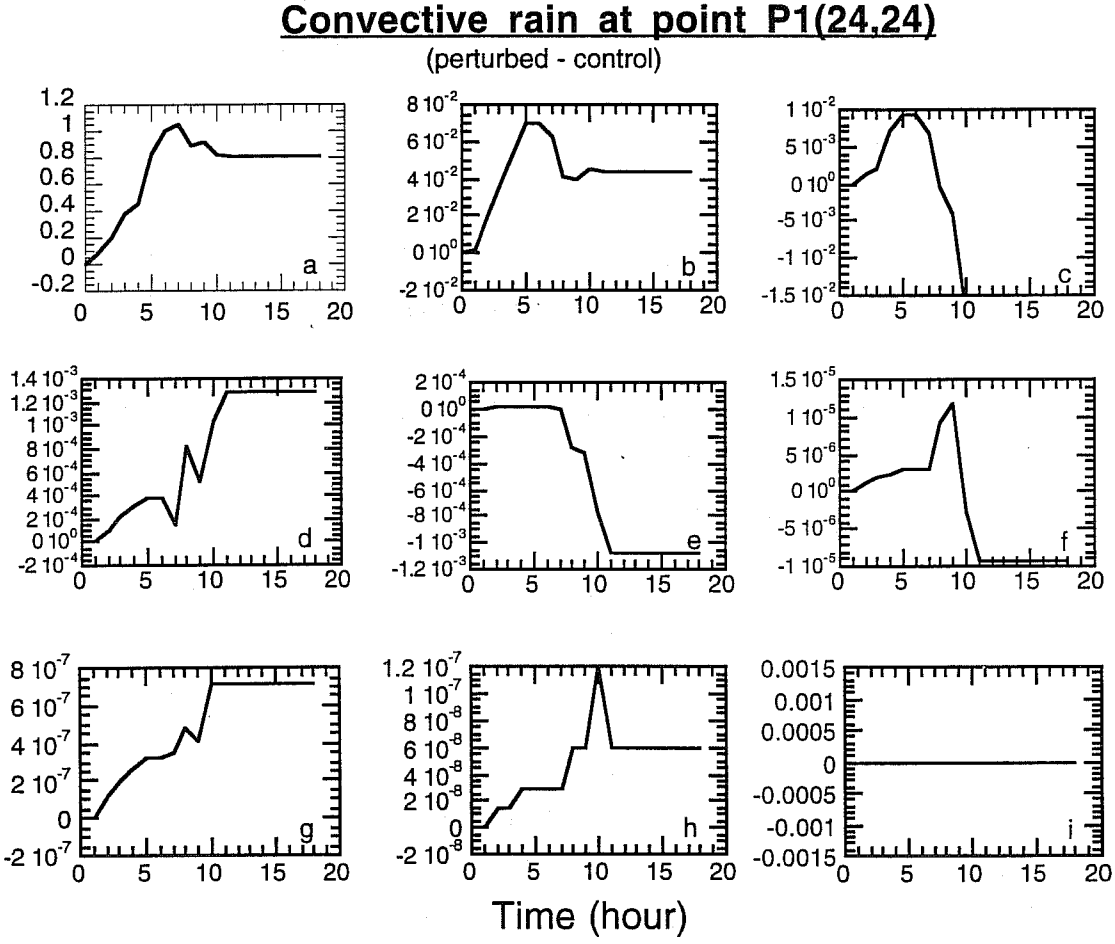

Figure 14: The time evolution of the perturbed hourly convective rainfall difference for experiments (a) E.10^0, (b) E.10^{-1}, ..., and (i) E.10^{-7} at the same point as in Fig. 13.

although the initial perturbation can be very small.

4.2 Impact of infrequent basic-state update to the accuracy of TLM solution

As mentioned in Section 5.1, the MM5 TLM and adjoint models can be used for many applications. Since the TLM is a model linearized around the nonlinear model solution in time, the MM5 model solution at every time step has to be saved and then inputs to both the TLM and the adjoint model. This may present a storage problem even for a medium-size job on current computers. For example, in a 6-h sensitivity study of the case with a grid-size of 62x79x27 and a time step of 1 min., the basic state saved from MM5 will need 6.07 GB disc space, almost reaching our current limit each user may have in his/her working directory. If one wishes to extend the sensitivity study to 12 h, it can be done only if there is a way, either to shift some of the nonlinear model output to other places such as to the mass storage during the job excution time, or to use an infrequent update of the basic state for TLM and the adjoint model. In the following, we will explore the possibility of using an infrequent update and examine the accuracy change of the TLM solutions with various basic state update lengths. Results will be presented for the moist case in which the convection related "on-off" switch is a factor to consider. A similar accuracy test of a dry TLM was carried out by Errico et al. (1993).

The same case as that used in Section 3 is used for these tests in order to test both the moist TLMs due to the strong convective activity and heavy rainfall of this case. Strong feedback from cumulus convection to the model fields can be expected.

Figure 15 shows the rms errors of a moist TLM approximation for a 30-min (thin solid line), 1.5-h (dashed line), and 3-h (dotted line) for all the model fields, compared with the same TLM solution with the exact basic state at every time step. As a reference, we also plotted the rms errors of the dry TLM approximation with a 1.5-h update (thick solid line). A linear interpolation scheme is used for the basic state calculation. We found that the rms errors are doubled if the basic-state update length is doubled. The error growth of a TLM with infrequent update is much larger when moist processes are included. The error evolution from the dry TLM integration is still characterized by the large initial error growth, and the errors in each field after about 4-h integration are kept constant in time with the exception of the specific humidity field. This is partly associated with the sweeping effect of the unperturbed lateral boundary conditions and partly with

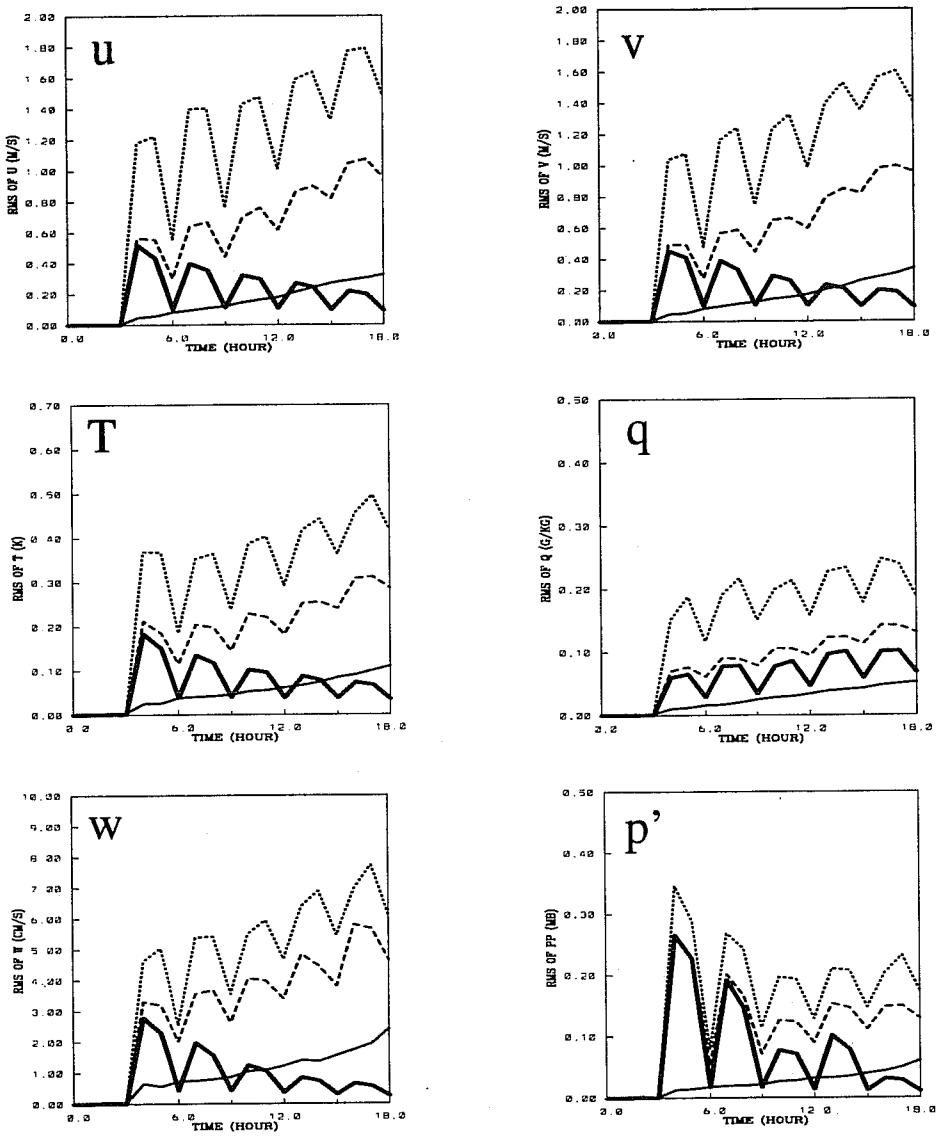

Figure 15: The rms errors of the TLM approximation including moist physics with a 30-min (thin solid line), 1.5-h (dashed line), and 3-h (dotted line) for all the model fields, compared with the corresponding TLM solution with the exact basic state at every time step. Also plotted in the figure is the rms errors of the dry TLM approximation with a 1.5-h update (thick solid line). A linear interpolation scheme is used for all of the basic state calculation.

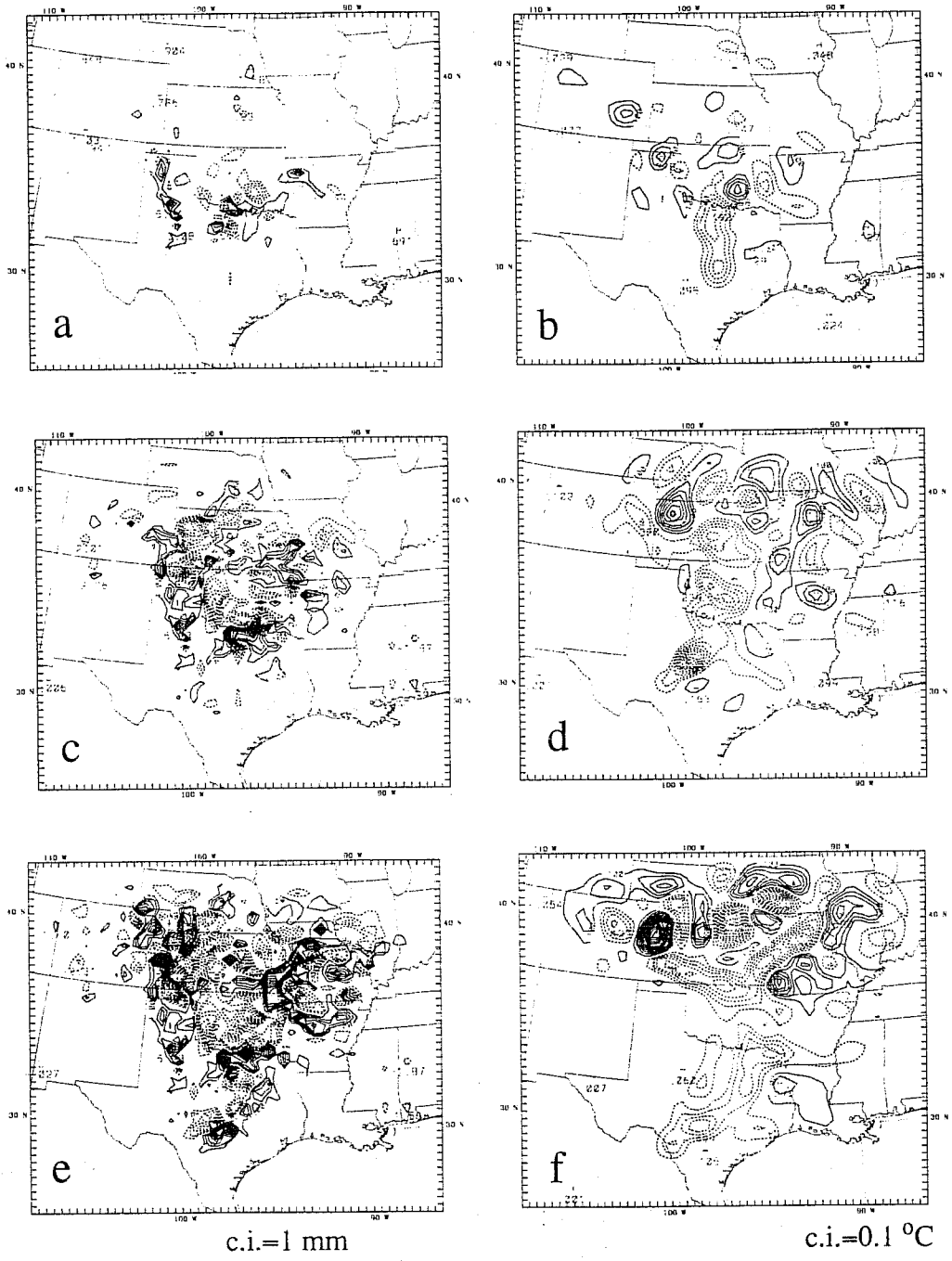

Figure 16: The errors in the 6-h rainfall (left column) and 850-mb temperature field (right column) at 0000 UTC 11 (a-b), 0600 UTC 11 (c-d), and 1200 UTC 11 April (e-f) for the experiment with 1.5 hour update frequency using a TLM including moist physics. Contour intervals are 1 mm for the 6-h rainfall and 0.1°C for the 850-mb temperature field.

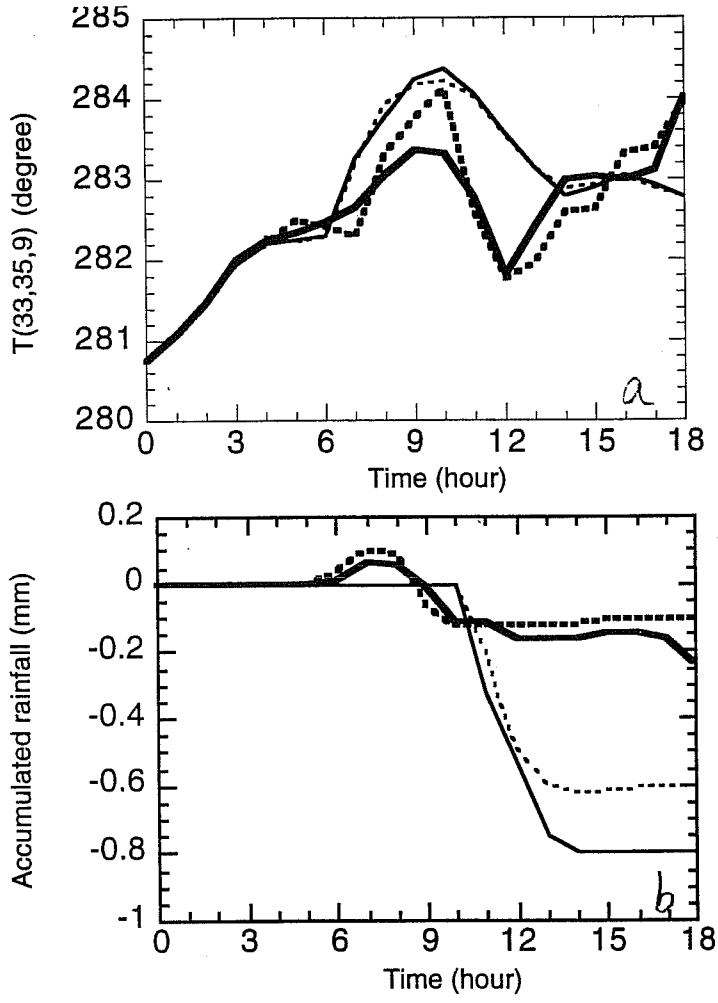

Figure 5.17: The time evolution of (a) the TLM solution of temperature with (thick lines) and without (thin lines) moist physics, and (b) the accumulated convective (thick lines) and nonconvective (thin lines) individual point (i=33,j=35,k=9). The solid lines are results obtained using an accurate basic state and the dashed lines are results with a 1.5-h update period.

the weaker nonlinearity in the adiabatic model, mostly advection. However, when moist physical processes are included, a much more pronounced error growth in time is observed. It can be related either to an over or an under prediction of the perturbed rainfall amount due to the presence of the basic-state determined "on-off" switches for precipitation to occur, or to the strong nonlinearity contained in the moist physics. Fig. 16 shows the errors in the 6-h rainfall (including both convective and nonconvective rain, left columns) and 850-mb temperature field (right columns) at 0000 UTC 11 (Figs. 16a,b), 0600 UTC 11 (Figs. 16c,d), and 1200 UTC 11 April (Figs. 16e,f) for the experiment with 1.5 hour update frequency. The error patterns in the 850-mb temperature fields are very similar to those in the precipitation fields at different times. If we examine the time evolution of the perturbed temperature at an individual point say (i=33,j=35,k=9), we find that the moist run produced a less smooth curve than the dry run (Fig. 17), and the same 1.5-h update frequency for a moist TLM produced a worse approximation (thick dashed line) to the accurate TLM solution (thick solid line) than a dry TLM (thin lines). If we examine the time evolution of the accumulated convective (thick lines) and nonconvective (thin lines) rainfall (Fig. 16b), we believe that the poor accuracy of a moist TLM is a result of the strong nonlinearity in the moist physical schemes, and not so much related to the presence of the basic-state determined "on-off" switches for precipitation to occur. This is because that the difference in the variation of precipitation switches between the TLM solutions with every time step basic state and with a 30-min update and a linear interpolation scheme are much smaller that the fifference in the precipitation amount between the two solutions. We examined several other convective points, randomly chosen, and same results are obtained.

The last accuracy test we made to the moist TLM solution with infrequent update is to keep the switches at every time step the same as in the true TLM while the nonlinear coefficients are approximately calculated. The accuracy is even worse than if both the switches and the nonlinear coefficients are approximately calculated and consistent.

5. Discusions

A nonhydrostatic mesoscale adjoint model has been developed which is suitable for many synoptic and mesoscale studies for a wide variety of problems requiring adjoint techniques. The adjoint model has been developed and coded based on the Penn State/NCAR

mesoscale model version 5 (MM5), and faithfully following the original MM5 code. A backward in time integration of the MM5 adjoint model produces an accurate gradient of any forecast aspect in a computationally efficient way.

Preliminary experiments of data assimilation were described to test the computational aspects of the MM5 adjoint model. The accuracy of the TLM, on which the adjoint model code is based, was examined in a convective case. The specific problem in the rainfall data assimilation associated with the "on-off" switches in the observation operator was addressed.

The 4DVAR, with adjoint physics, was capable of fitting the model to the observed rainfall observation. The forecast starting from the 4DVAR-modified IC produced an improved short-range prediction of convection. Further improvement using more complex adjoint physical processes was found to be marginal. Limitation in the rainfall assimilation using 4DVAR due to the dependence of the rain observation operators on the basic-state determined "on-off" switches was shown to exist. Observed rainfall over a model no-rain region may have no impact on the 4DVAR results, depending on whether or not there are other observations which can adjust the model IC with which the new model forecast will produce precipitation during the entire minimization procedure.

A careful examination of the nonlinearity of dry and moist versions of MM5 was conducted using the 4DVAR derived "optimal" perturbations at the initial time. The size of the perturbation was similar or slightly larger than the current analysis errors. Strong nonlinear behavior was observed for very small perturbations in IC, i.e., the order of magnitude was as small as 10^{-4} for wind (m/s), temperature (^{o}C), and specific humidity (g/kg). The dry version of MM5 showed a consistent linear behavior as the order of magnitude of the initial perturbation was decreased.

Although the dry TLM are exactly asymptotic to the true nonlinear perturbation solution determined as differences between nonlinear calculations, even for perturbations as large as current analysis errors, a moist TLM didn't produce a similarly good approximation to the nonlinear perturbation solution for those initial perturbations, which were very small in magnitude but sufficient to produce a different rainfall prediction than that in the control forecast.

In a test of using an infrequent basic-state update, we found that 1.5-h was a suitable update period for a dry TLM and a 30-min update was suitable for a moist TLM. With these update frequencies, the rms errors for the 18-h forecast was less than 0.5 m/s for the wind, 0.2^o C for the temperature, 0.1 g/kg for the specific humidity, 3 cm/s for the vertical velocity, and 0.3 mb for the pressure perturbation fields. A delayed infrequent update was suggested due to the presence of gravity oscillations at the first few hours of model integration without initialization.

REFERENCES

Errico, R. M., T. Vukićević, and K. Raeder, 1993: Examination of the accuracy of a tangent linear model. *Tellus*, **45A**, 462-477.

Grell, G. A., Dudhia, J. and Stauffer D. R. 1994. A description of the fifth-generation Penn State/NCAR mesoscale model (MM5). *NCAR Technical Note* , NCAR/TN-398 + STR, National Center for Atmospheric Research, Boulder, CO, 138 pp.

Xu, Q., 1996: Generalized adjoint for physical processes with parameterized discontinuities - Part I: Basic issues and heuristic examples. *J. Atmos. Sci.*, **53**, 1123-1142.

Zou, X., 1996: Tangent linear and adjoint of "on-off" processes and their feasibility for use in four-dimensional variational data assimiolation. *Tellus*, **49A**, 3-31.

Zou, X. and Kuo, Y.-H., 1996: Rainfall assimilation through an optimal control of initial and boundary conditions in a limited-area mesoscale model. *Mon. Wea. Rev.*, **124**, 2859-2882.

Zou, X., Kuo, Y.-H. and Guo, Y.-R. 1995. Assimilation of atmospheric radio refractivity using a nonhydrostatic adjoint model. *Mon. Wea. Rev.* **123**, 2229-2249.